Fluorescence Polarization Anisotropy in Microdroplets

Zhenpeng Zhou, Xin Yan, Yin-Hung Lai, and Richard N. Zare*

Department of Chemistry, Stanford University, Stanford, California 94305, United States

Ⓢ *Supporting Information*

ABSTRACT: Chemical reactions can be greatly accelerated in microdroplets, but the factors that lead to acceleration are still being elucidated. Using rhodamine 6G (R6G) as a model compound, we studied the density distribution and fluorescence polarization anisotropy of this dye in water-in-oil microdroplets. We found the density of R6G is higher on the surface of the microdroplets, and the ratio of the surface density to that of the center grows with increasing microdroplet radius or with decreasing R6G concentration. The measured fluorescence polarization anisotropy at the surface is almost the same for droplets of different sizes but becomes larger when the concentration is lowered. We also performed three-dimensional simulations by treating $R6G^+$ and its associated anion as a dipole of fixed length and magnitude. The simulation results match quite well the experimental measurements, showing that the density distribution and fluorescence polarization anisotropy can be largely explained by a simple electrostatic model.
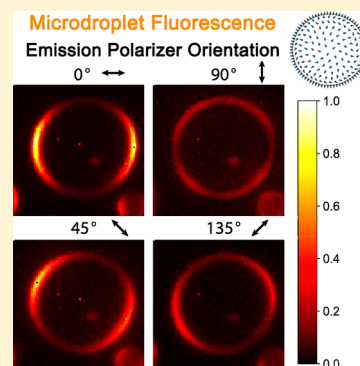
Chemical reactions happening within microdroplets have received much attention in recent years. Researchers from various groups have shown that numerous reactions can be accelerated in microdroplets compared with their counterparts in the bulk phase, including protein unfolding,[1] helix formation,[2] synthesis of sugar phosphates and ribonucleosides,[3,4] addition−condensation reactions,[5−9] C−C and C−N bond formation reactions,[8,10,11] radical reactions,[12,13] and nanostructure formations.[14] However, the causes of reaction acceleration in microdroplets remain to be fully elucidated. There have been multiple hypotheses concerning the factors that contribute to reaction acceleration, including solvent evaporation and in situ acidity or basicity.[15−18] In addition, researchers have done simulations in a much smaller nanometer scale for reactions happening in water confined by mineral surfaces.[19] In extension of those efforts, we measured the physical properties, i.e., the density distribution and the polarization anisotropy of rhodamine 6G (R6G) fluorescence in water-in-oil microdroplets to facilitate an understanding of microdroplet chemistry in a more quantitative way.

What makes microdroplets different from the bulk solution is mainly the large surface area and a confined space. The properties of molecules on the surface have been studied for the oil/water,[20−22] air/water,[23−27] and silica/water[28,29] interfaces. Most of this work has been done for an interface that constitutes an open surface, which is bounded by one or more edges. Here we studied the density distribution and fluorescence polarization anisotropy of R6G at the oil−water interface that constitutes a closed surface, which is compact and without boundary. With the assumption that the angle between the adsorption dipole and emission dipole is close to zero,[30] the fluorescence polarization anisotropy is defined in eq 1, where $I_\parallel$ denotes the fluorescence intensity when the emission polarizing filter is oriented in the same direction as the excitation filter, while $I_\perp$ denotes the fluorescence intensity when they are perpendicular.

$$A = \frac{I_\parallel - I_\perp}{I_\parallel + 2I_\perp}$$

(1)

In our experimental setup, a focused flow droplet generator was used to generate water-in-oil microdroplets. As a model system, a R6G−water solution was used as the water phase and Fluorinert FC-40 was used as the oil phase. A modified epifluorescence microscope setup was used to measure the polarization anisotropy in microdroplets. (Scheme 1) The

Scheme 1. Schematic View of the Experimental Setup
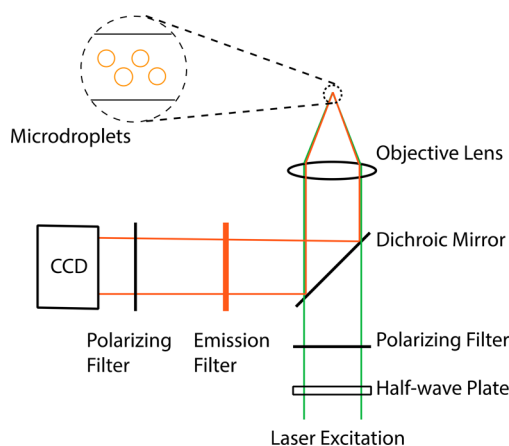
excitation laser was passed through a half-wave plate to shift the direction of linearly polarized light, then through a polarizing filter, and then focused by an objective lens. The fluorescence of

R6G went through an emission filter and a polarizing filter, followed by detection with a CCD sensor. The fluorescence measurement was done after the system reached an equilibrium (Figure S1).

Figure 1 presents images of the fluorescence from a microdroplet. The dye molecules of R6G concentrate more at
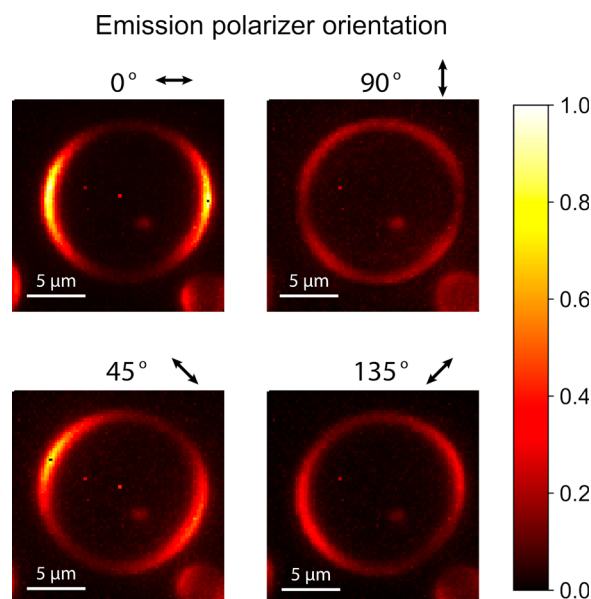
Emission polarizer orientation

Figure 1. Fluorescence intensity of a microdroplet for different excitation–detection conditions. The linear polarization of the excitation filter was fixed horizontally at 0°, while the linear polarization of the emission filter was set at 0°, 45°, 90°, or 135°.

and near the surface than in the center of the microdroplet. The excitation polarizing filter was fixed horizontally at 0°, while the emission polarizing filter was set at 0°, 45°, 90°, or 135°. The images show the intensity change of different parts of the microdroplet for different orientations of the emission filter polarizer. Specifically, when the emission polarizer was placed at 90°, the top, bottom, left, and right parts of the microdroplet are darker than the other parts. The top and bottom parts are dark because the excitation filter was placed horizontally, and the top and bottom parts are not excited, while the darkness of the left and

right parts comes from the fact that the emission polarizer was placed vertically at 90°, and the fluorescence is blocked by this filter. These images indicate that the emission dipoles of the molecules at the surface of the microdroplet are perpendicular to the surface.

Figure 2A shows that the fluorescence polarization anisotropy (eq 1) increases as the fractional distance of molecules to the center increases. We conclude from this behavior that molecules at the surface are more aligned. The fluorescence anisotropy of different sized microdroplets shows similar trends. Figure 2B shows that the fluorescence polarization anisotropy at the surface of different sized microdroplets with the same R6G concentration is similar and that microdroplets with lower concentrations have higher values of the fluorescence polarization anisotropy at the surface. As control experiments, the fluorescence polarization anisotropy of 1 μM R6G was measured to be 0.014 in bulk solution and 0.043 at a flat open water−oil interface. The latter experiment shows that the hydrophobic−hydrophilic interaction is not the main cause for the anisotropy at the microdroplet surface. We reason that if the hydrophobic−hydrophilic interaction were the main cause for anisotropy, the anisotropy at the microdroplet surface and an open surface would be similar, as they both have oil−water interfaces. We propose that the anisotropy of R6G is caused by electrostatic interactions in a space confined by a closed surface.

A confocal microscope without polarizing filter was used to take an image at the largest cross section (great circle) of different sized microdroplets with R6G at concentrations of 1, 10, and 1000 μM. Figure 3A shows the normalized fluorescence intensity as a function of the fractional distance from the center. The fluorescence intensity shows a strong variation from the center to the surface of the microdroplets. For microdroplets with different sizes (6−28 μm), the surface density of R6G is higher than that in the center. However, the surface-to-center density ratio decreases with higher concentrations of R6G or with smaller microdroplet sizes (Figure 3B). To explain the above observations, we hypothesized that the higher concentration of R6G molecules on the surface than at the center of the microdroplets comes from the electrostatic repulsion of the dipoles. There is a maximum capacity of the microdroplet surface, because all molecules take a specific volume. Thus, for smaller microdroplets or those with higher concentrations, the surface is largely occupied, and excess
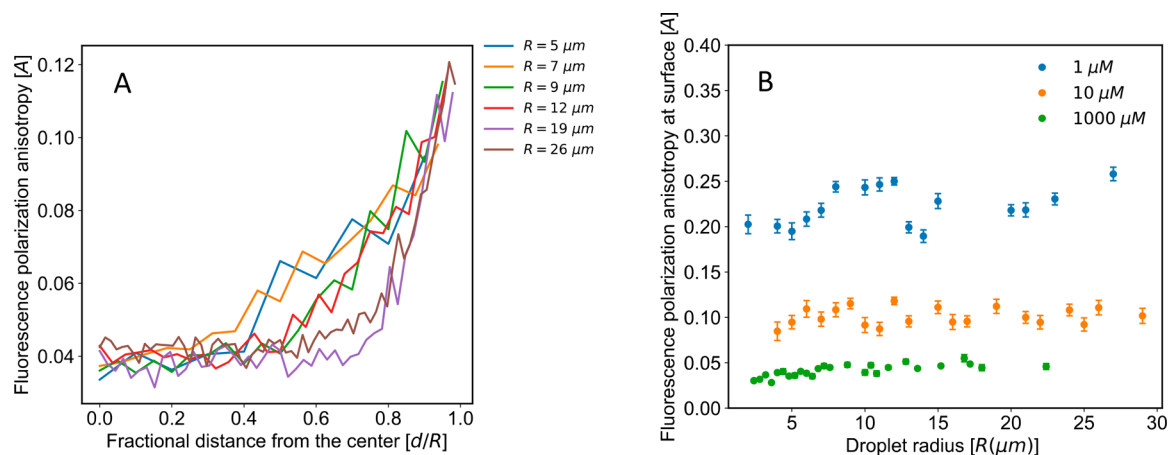

Figure 2. (A) Fluorescence polarization anisotropy (eq 1) as a function of fractional distance from the center of microdroplets, where d is the distance from the center and R is the radius of the droplet. The concentration of R6G is 10 μM. (B) The fluorescence polarization anisotropy at the surface for different sized droplets with various concentrations of R6G. The thickness of the surface used in the analysis is 2 μm. The error bars represent one standard deviation.
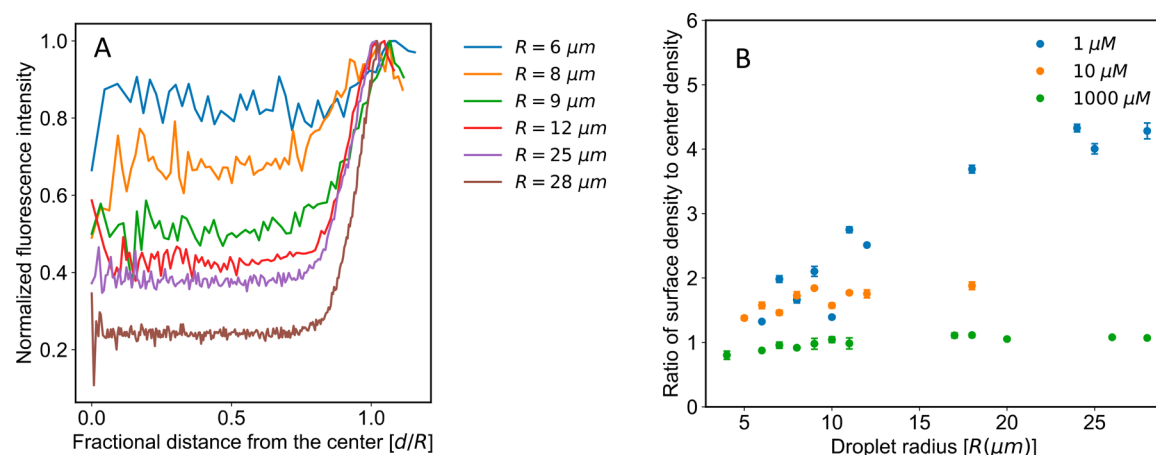
Figure 3. (A) Relative fluorescence intensity versus the fractional distance from the center, where d is the distance from the center and R is the radius of the droplet. The concentration of R6G is 1 μM. (B) The surface-to-center density ratios for different droplet sizes and different concentrations. The thickness of the surface used in the analysis is 2 μm. The error bars represent one standard deviation.

molecules can only stay closer to the center. Therefore, the ratio of the surface density to that of the center was lower for smaller microdroplets or higher concentrations of R6G.

To investigate the cause of anisotropy at the surface, a three-dimensional simulation was implemented by considering the positively charged R6G and its negatively charged counterion as a dipole of fixed length and magnitude. The translational and rotational motion of the dipole at each time step was calculated by solving the ordinary differential equation described by eq 2:

$$\frac{\mathrm{d}}{\mathrm{d}t}\mathbf{S}(t) = \frac{\mathrm{d}}{\mathrm{d}t}\begin{pmatrix} \mathbf{x}(t) \\ \mathbf{q}(t) \\ \mathbf{p}(t) \\ \mathbf{L}(t) \end{pmatrix} = \begin{pmatrix} \mathbf{v}(t) \\ \frac{1}{2}\boldsymbol{\omega}(t)\,\mathbf{q}(t) \\ \mathbf{F}(t) \\ \mathbf{M}(t) \end{pmatrix}$$

$$\mathbf{F}_i = -\sum_{j \neq i}^{N} \frac{\mathbf{r}_{ij}}{r_{ij}^3}$$

$$\mathbf{p}(t) = \sum m_i \mathbf{v}(t)$$

$$\mathbf{F}(t) = \sum \mathbf{F}_i(t)$$

$$\mathbf{L}(t) = \mathbf{I}(t)\boldsymbol{\omega}(t)$$

$$\mathbf{M}(t) = \sum \left(\mathbf{r}_i(t) - \mathbf{x}(t)\right) \times \mathbf{F}_i(t) \tag{2}$$

where $\mathbf{x}$ is the positional vector of the dipole, $\mathbf{v}$ the linear velocity, $\mathbf{q}$ the quaternion representing the dipole rotation, $\boldsymbol{\omega}$ the angular velocity, $\mathbf{F}_i$ the electric force, $\mathbf{r}_{ij}$ the distance from the ith and jth particles, and N the total number of particles; r_{ij} denotes scalar distance between the ith and jth particles; $\mathbf{p}$ is the linear momentum, $\mathbf{L}$ the angular momentum, $\mathbf{I}$ the inertia tensor, and $\mathbf{M}$ the torque. The location of the dipoles is restricted to lie within the water droplet sphere. The whole procedure was repeated until the total energy converged. Figure 4A shows a sample simulation result. The dipoles located at the outmost boundary of the sphere are perpendicular to the surface, which confirms our findings in Figure 1. One hundred simulations with different initial dipole positions were made separately. Figure 4C compares the average density distribution in 100 simulations and that in experiments, indicating that the uneven distribution of molecules in the

microdroplets is mainly from electrostatic repulsion. We propose the variance of dipole angles is a measurement for the randomness of orientation of molecules, while the fluorescence polarization anisotropy is higher where the randomness of molecules is lower. Thus, we calculated the variance of the dipole orientations and plotted the reciprocal of variance from simulation and the fluorescence anisotropy from experiment in Figure 4D. They agree closely. The orientation of dipoles in the second outmost layer is more random than that in the outmost layer. Because of the diffraction limit, the measurement we made about the surface is affected by several layers of molecules inside, and we should expect less influence from inner layers at lower concentrations. This explains the experimental results that microdroplets with lower concentrations will have higher observed anisotropy, as shown in Figure 2.

We believe our investigation of the density distribution and fluorescence anisotropy of microdroplets sheds light on answering the question of why reactions in microdroplets differ from reactions in the bulk phase.[31] First, from the concentration prospective, greater density leads to greater reaction rate. For smaller microdroplets, the ratio of the surface density to that of the center is lower, which is caused by the fact that the center density of smaller microdroplets is greater, while the surface densities are similar for different sized droplets. Therefore, from the concentration perspective, we expect larger reaction rate acceleration in smaller microdroplets. In addition, in smaller droplets, diffusion allows more mixing of molecules located on the inside and the periphery of the droplet, which leads to an increased rate of reaction for the whole droplet. Second, from the polarization anisotropy perspective, as molecules are aligned (ordered), their entropies are reduced, which can affect the free-energy change for the reaction.

■ EXPERIMENTAL SECTION

All chemicals were purchased as MS grade from Sigma-Aldrich (St. Louis, MO). The focus-flow droplet generator chip was purchased from Micronit Microfluidics (Netherlands). The fluorescence anisotropy was measured with a Nikon TE-2000 inverted fluorescence microscope. The fluorescence intensity of cross sections of microdroplets was measured with a Leica TCS SP2 confocal microscope.

In the concentration distribution and fluorescence anisotropy measurement, an image was taken at the largest cross section of a
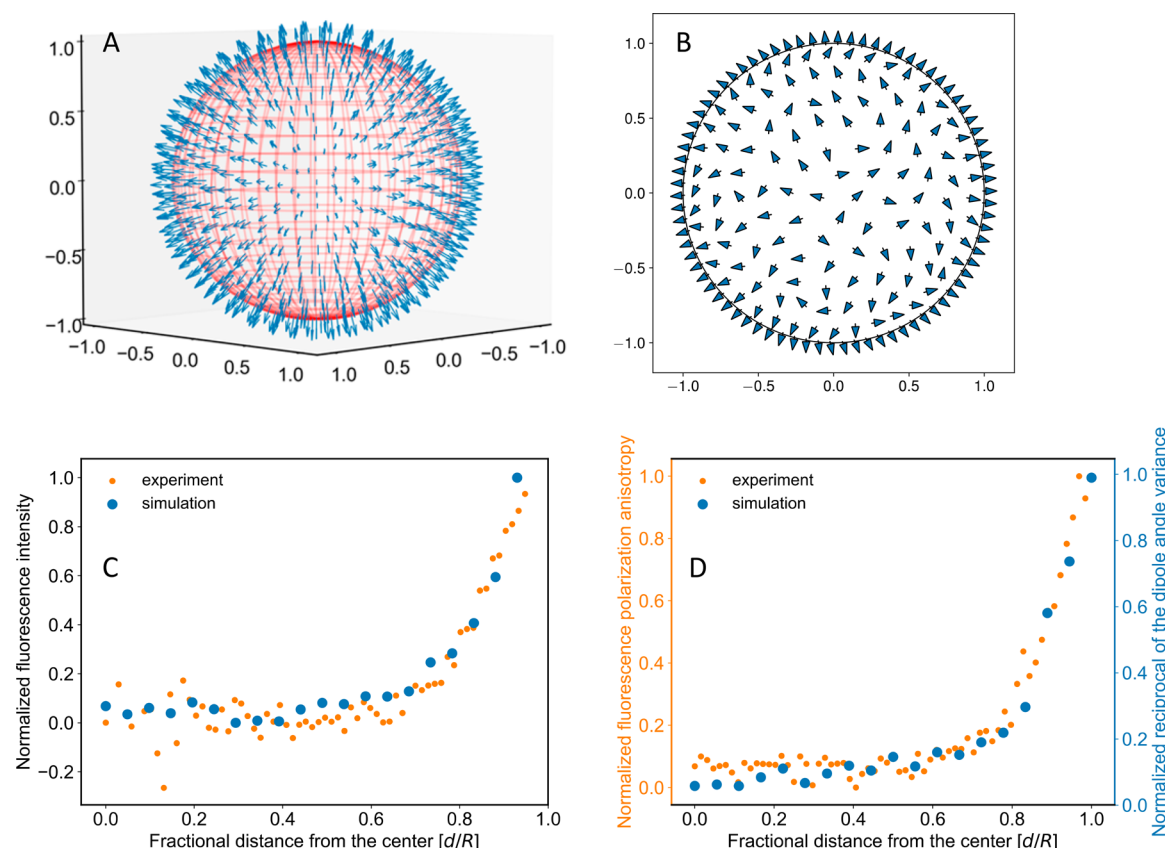
Figure 4. (A) A sample simulation result considering dipole−dipole interaction, with the number of dipoles being 600. The arrows show the directions of dipoles. (B) An illustration of the simulation result in two dimensions. (C) Comparison of the three-dimensional simulation result (blue dots) with the experimental data (orange dots). The microdroplet size was 9 μm, and the concentration of R6G was 1 μM. (D) Comparison of the simulated reciprocal of the dipole angle variance against the experimental fluorescence anisotropy.

microdroplet after 10 min of stabilization. The fluorescence measurement was done after the system reached an equilibrium (Figure S1). In the density distribution measurement, the optical resolution was reported to be 500 nm, while in the anisotropy study, the resolution was reported to be 1200 nm.

The intensity information at each point was extracted as a vector of (d, θ, I), where (d, θ) is the polar coordinate for the point and I is the intensity. Furthermore, the intensity was averaged across θ for each d, resulting in a relationship between I and d.

The simulation was done by a hand-written code using the framework of mxnet.[32] The time step Δt was set to be 1×10^{-7}, and the total number of steps is 1×10^{7}. The length of the dipoles was set to be 0.001. Those values are relative ones without units with respect to the Coulomb constant $k_e = 1$ and the radius of a microdroplet $R = 1$.

ASSOCIATED CONTENT

Ⓢ Supporting Information

The Supporting Information is available free of charge on the ACS Publications website at DOI: 10.1021/acs.jpclett.8b01129.

Polarization imaging as a function of time (PDF)

AUTHOR INFORMATION

ORCID Ⓘ

Zhenpeng Zhou: 0000-0002-3282-9468
Yin-Hung Lai: 0000-0003-4245-2016
Richard N. Zare: 0000-0001-5266-4253

REFERENCES

(1) Lee, J. K.; Banerjee, S.; Nam, H. G.; Zare, R. N. Acceleration of Reaction in Charged Microdroplets. *Q. Rev. Biophys.* **2015**, *48*, 437−444.

(2) Mortensen, D. N.; Williams, E. R. Microsecond and Nanosecond Polyproline II Helix Formation in Aqueous Nanodrops Measured by Mass Spectrometry. *Chem. Commun. (Cambridge, U. K.)* **2016**, *52*, 12218−12221.

(3) Nam, I.; Lee, J. K.; Nam, H. G.; Zare, R. N. Abiotic Production of Sugar Phosphates and Uridine Ribonucleoside in Aqueous Microdroplets. *Proc. Natl. Acad. Sci. U. S. A.* **2017**, *114*, 12396−12400.

(4) Nam, I.; Nam, H. G.; Zare, R. N. Abiotic Synthesis of Purine and Pyrimidine Ribonucleosides in Aqueous Microdroplets. *Proc. Natl. Acad. Sci. U. S. A.* **2018**, *115*, 36−40.

(5) Bain, R. M.; Pulliam, C. J.; Thery, F.; Cooks, R. G. Accelerated Chemical Reactions and Organic Synthesis in Leidenfrost Droplets. *Angew. Chem., Int. Ed.* **2016**, *55*, 10478−10482.

(6) Bain, R. M.; Pulliam, C. J.; Cooks, R. G. Accelerated Hantzsch Electrospray Synthesis with Temporal Control of Reaction Intermediates. *Chem. Sci.* **2015**, *6*, 397−401.

(7) Girod, M.; Moyano, E.; Campbell, D. I.; Cooks, R. G. Accelerated Bimolecular Reactions in Microdroplets Studied by Desorption Electrospray Ionization Mass Spectrometry. *Chem. Sci.* **2011**, *2*, 501−510.

(8) Bain, R. M.; Sathyamoorthi, S.; Zare, R. N. On-Droplet" Chemistry: The Cycloaddition of Diethyl Azodicarboxylate and Quadricyclane. *Angew. Chem., Int. Ed.* **2017**, *56*, 15083−15087.

(9) Lai, Y.-H.; Sathyamoorthi, S.; Bain, R. M.; Zare, R. N. Microdroplets Accelerate Ring Opening of Epoxides. *J. Am. Soc. Mass Spectrom.* **2018**, *29*, 1036−1043.

(10) Badu-Tawiah, A. K.; Campbell, D. I.; Cooks, R. G. Accelerated C-N Bond Formation in Dropcast Thin Films on Ambient Surfaces. *J. Am. Soc. Mass Spectrom.* **2012**, *23*, 1461−1468.

(11) Müller, T.; Badu-Tawiah, A.; Cooks, R. G. Accelerated Carbon-Carbon Bond-Forming Reactions in Preparative Electrospray. *Angew. Chem., Int. Ed.* **2012**, *51*, 11832−11835.

(12) Lai, Y.-H.; Zhou, Z.; Basheer, C.; Zare, R. N. Upgrading Asphaltenes by Oil Droplets Striking a Charged TiO_2 -Immobilized Paper Surface. *Energy Fuels* **2017**, *31*, 12685−12690.

(13) Houle, F. A.; Wiegel, A. A.; Wilson, K. R. Changes in Reactivity as Chemistry Becomes Confined to an Interface. the Case of Free Radical Oxidation of $C_{30}H_{62}$ Alkane by OH. *J. Phys. Chem. Lett.* **2018**, *9*, 1053−1057.

(14) Guardingo, M.; Busqué, F.; Ruiz-Molina, D. Reactions in Ultra-Small Droplets by Tip-Assisted Chemistry. *Chem. Commun. (Cambridge, U. K.)* **2016**, *52*, 11617−11626.

(15) Fallah-Araghi, A.; Meguellati, K.; Baret, J.-C.; El Harrak, A.; Mangeat, T.; Karplus, M.; Ladame, S.; Marques, C. M.; Griffiths, A. D. Enhanced Chemical Synthesis at Soft Interfaces: A Universal Reaction-Adsorption Mechanism in Microcompartments. *Phys. Rev. Lett.* **2014**, *112*, 028301.

(16) Jacobs, M. I.; Davies, J. F.; Lee, L.; Davis, R. D.; Houle, F.; Wilson, K. R. Exploring Chemistry in Microcompartments Using Guided Droplet Collisions in a Branched Quadrupole Trap Coupled to a Single Droplet, Paper Spray Mass Spectrometer. *Anal. Chem.* **2017**, *89*, 12511−12519.

(17) Mondal, S.; Acharya, S.; Biswas, R.; Bagchi, B.; Zare, R. N. Enhancement of Reaction Rate in Small-Sized Droplets: A Combined Analytical and Simulation Study. *J. Chem. Phys.* **2018**, submitted for publication.

(18) Yan, X.; Bain, R. M.; Cooks, R. G. Organic Reactions in Microdroplets: Reaction Acceleration Revealed by Mass Spectrometry. *Angew. Chem., Int. Ed.* **2016**, *55*, 12960−12972.

(19) Muñoz-Santiburcio, D.; Marx, D. Chemistry in Nanoconfined Water. *Chem. Sci.* **2017**, *8*, 3444−3452.

(20) Ishizaka, S.; Kitamura, N. Time-Resolved Total Internal Reflection Fluorometry Study on Chemical and Structural Characteristics at Water/Oil Interfaces. *Bull. Chem. Soc. Jpn.* **2001**, *74*, 1983−1998.

(21) Osakai, T.; Yamada, H.; Nagatani, H.; Sagara, T. Potential-Dependent Adsorption of Amphoteric Rhodamine Dyes at the Oil/Water Interface as Studied by Potential-Modulated Fluorescence Spectroscopy. *J. Phys. Chem. C* **2007**, *111*, 9480−9487.

(22) Chen, V.; Warr, G. G.; Evans, D. F.; Prendergast, F. G. Curvature and Geometric Constraints as Determinants of Microemulsion Structure: Evidence from Fluorescence Anisotropy Measurements. *J. Phys. Chem.* **1988**, *92*, 768−773.

(23) McConnell, H. M. Structures and Transitions in Lipid Monolayers at the Air-Water Interface. *Annu. Rev. Phys. Chem.* **1991**, *42*, 171−195.

(24) Moy, V. T.; Keller, D. J.; McConnell, H. M. Molecular Order in Finite Two-Dimensional Crystals of Lipid at the Air-Water Interface. *J. Phys. Chem.* **1988**, *92*, 5233−5238.

(25) Castro, A.; Sitzmann, E. V.; Zhang, D.; Eisenthal, K. B. Rotational Relaxation at the Air/Water Interface by Time-Resolved Second Harmonic Generation. *J. Phys. Chem.* **1991**, *95*, 6752−6753.

(26) Eisenthal, K. B. Liquid Interfaces Probed by Second-Harmonic and Sum-Frequency Spectroscopy. *Chem. Rev.* **1996**, *96*, 1343−1360.

(27) Eisenthal, K. B. Liquid Interfaces. *Acc. Chem. Res.* **1993**, *26*, 636−643.

(28) Chen, Z.; Tang, Y. J.; Xie, T. T.; Chen, Y.; Li, Y. Q. Fluorescence Spectral Properties of Rhodamine 6G at the Silica/Water Interface. *J. Fluoresc.* **2008**, *18*, 93−100.

(29) Wirth, M. J.; Burbage, J. D. Adsorbate Reorientation at a Water/(Octadecylsilyl)Silica Interface. *Anal. Chem.* **1991**, *63*, 1311−1317.

(30) Zare, R. N. *Angular Momentum: Understanding Spatial Aspects in Chemistry and Physics*; 1st ed.; Wiley, 1991.

(31) Banerjee, S.; Gnanamani, E.; Yan, X.; Zare, R. N. Can All Bulk-Phase Reactions Be Accelerated in Microdroplets? *Analyst* **2017**, *142*, 1399−1402.

(32) Chen, T.; Li, M.; Li, Y.; Lin, M.; Wang, N.; Wang, M.; Xiao, T.; Xu, B.; Zhang, C.; Zhang, Z. MXNet: A Flexible and Efficient Machine Learning Library for Heterogeneous Distributed Systems. arXiv.org, **2015**, http://arxiv.org/abs/1512.01274.